Spatial Charge Configuration Regulates Nanoparticle Transport and Binding Behavior In Vivo

Published in final edited form as:
Angew Chem Int Ed Engl. 2013 January 28; 52(5): 1414–1419. doi:10.1002/anie.201208331.

Spatial charge configuration regulates nanoparticle transport and binding behavior *in vivo*

Hee-Sun Han[1], **John D. Martin**[2,3], **Jungmin Lee**[1], **Daniel K. Harris**[4], **Dai Fukumura**[2], **Rakesh K. Jain**[2], and **Moungi Bawendi**[1,*]

[1]Department of Chemistry, Massachusetts Institute of Technology, Cambridge, MA 02139, USA

[2]Edwin L. Steele Laboratory, Department of Radiation Oncology, Massachusetts General Hospital and Harvard Medical School, Boston, MA 02114, USA

[3]Department of Chemical Engineering, Massachusetts Institute of Technology, Cambridge, MA 02139, USA

[4]Department of Materials Science and Engineering, Massachusetts Institute of Technology, Cambridge, MA 02139, USA

Abstract

Detailed Charge arrangements: A new set of zwitterionic quantum dots were synthesized and used to study the influence of microscopic charge arrangements on the *in vivo* behavior of nanoparticles. Experiments using cultured cells and live mice demonstrate that the microscopic arrangement of surface charges strongly influence nonspecific binding, clearance behavior, and *in vivo* transport of nanoparticles.

Keywords

Cancer; Ligand design; Nanoparticles; Quantum dots; Zwitterions

Nanoparticles are widely used as imagingprobes[1] or as drug carriers[2], however, the design rules to guide theirproperties for *in vivo* application remain incomplete. Until recently, the physical characteristics of nanoparticles such as size, shape, hydrophobicity and net charge have been mostly considered as primary handles to achieve nanoparticles with desired *in vivo* characteristics. However, we hypothesized that the detailed arrangement of ligands also has a strong influence on the *in vivo* behavior of nanoparticlesbecause the interactions of nanoparticles with the surrounding biomolecules or cellular structures are mediated by surface-to-surface contacts. In support of this hypothesis, previous work has shown that specific arrangements of hydrophobic ligands on the nanoparticle surface can affect the cellular uptake pathway of the particles[3]. In particular, we demonstrate the influence of spatial distribution of surface charge on the binding and transport behavior of nanoparticles *in vivo*. Studying the influence of charge distribution on nanoparticle behavior is essential as most nanoparticle coatings employ charged functional groups for further conjugation with biomolecules or drugs. Even though there have been reports on nanoparticles employing uncharged functional groups for conjugations[4], most widely used conjugation methods still rely on ester bond formation, amide coupling, or maleimide-thiol coupling that utilize carboxylic acid or amine groups. In addition, studying the influence of surface charge arrangement on nanoparticle behavior inspires the design of zwitterionic

*Corresponding author: mgb@mit.edu.

surface coatings, which were recently introduced as possible alternative for bulky non-ionic polymeric surface coating such as polyethylene glycol (PEG)[5].

For this study, quantum dots (QDs) coated with newly designed betaine functionalized polyimidazole ligands (BPILs) were utilized. The unique optical properties of QDs[6] allow facile analysis of QD behavior using optical microscopes, rather than elemental analysis[7], magnetic resonance imaging[8], or electron microscopy[9], and simultaneous analysis of multiple targets. Recent advances in the development of non-ionic or charged surface coatings enabled preparation of high quality QDs in aqueous buffers[10]. However, most zwitterionic surface coatings for QDs that are currently reported employ thiol as a binding group[5a, 5b, 11], and thus suffer from poor stability in ambient condition owing to the oxidation of thiolsand significant nonspecific binding to serum proteins[10c, 11]. To prepare stable and biocompatible zwitterionic QDs, we designed new zwitterionic coatings containing multiple imidazole moieties, which are chemically stable, as cooperative binding groups to the QD surface. In addition to an enhanced solution stability, BPIL QDs have other potential advantages such as a compact size, a narrow polydispersity index of the polymer, straightforward modulation of charge density and charge distribution, and minimal nonspecific binding towards cells and proteins.

Betaine polyimidazole ligands (BPILs), random co-polymers employingimidazole groups for QD binding, and sulfobetaine (SBPILs) or carboxybetaine (CBPILs) groups for water solubilization, are synthesized *via* three steps (Scheme 1): (1) RAFT mediated polymerization of the backbone (**3**), (2) betainization of the polymers (**4**, **6**) and (3) cleavage of BOC protecting groups (**5**, **7**). RAFT mediated polymerization allows tight control over the mean and standard deviation of the resulting polymer weights, as shown in Supplementary Fig. S5. Post-modification of a polymerized backbone using highly strained 1,3-propane sultone and β-propiolactone enables one-step conversion of tertiary amines to sulfobetaineor carboxybetaine by releasing the ring strain. The net charge and degree of freely exposed amines of BPILs were controlled by tuning the conversion efficiencies of tertiary amines to betaine moieties.

Water soluble QDs coated with the BPILs (BPIL QDs) were prepared by exchanging the native hydrophobic ligands with BPILs. Various types of QDs ranging from the near infrared to the visible were successfully brought into water with both sulfobetaine functionalized polyimidazole ligands (SBPILs) and carboxybetaine functionalized polyimidazole ligands (CBPILs): InAs/CdZnS emitting at 750 nm ($QD_{\mathbf{750}}$), CdSe/CdS emitting at 570 nm ($QD_{\mathbf{570}}$) and CdSe/CdZnS emitting at 612 nm ($QD_{\mathbf{612}}$). Owing to multidentateimidazole binding units, BPIL QDs exhibit greatly enhanced stability across a wide pH range (Supplementary Fig. S10). In addition, both CBPIL and SBPIL QD solutions were stable under ambient conditions for over a month, which is a significant enhancement over the hours to days shelf lives of previously reportedzwitterionic QDs[5a, 5b]. Greatly enhanced stability of BPIL QDs allowed in-depth analysis of the *in vivo* behavior of zwitterionic QDs.

The net charge of SBPIL QDs and CBPIL QDs was characterized by measuring the zeta potential and by performing gel electrophoresis. The zeta potential of QDs coated with CBPIL with 100% conversion of tertiary amines to carboxybetaine moieties ($CBPIL_{100\%}$ QDs) was ~ 0.3mV (close to neutral) and that of $SBPIL_{100\%}$ QDs was ~ −13.1mV (mildly negatively charged) (Figure 1). The measured negative charge of SBPIL QDs, despite the zwitteronic nature of the SBPILs, can be explained by association of negative ions present in buffers with the quaternary amines in SBPILs (Supplementary results)[5e]. The net charge of SBPIL QDs was tuned by adjusting betainization efficiencies. As shown in Supplementary Table S1, neutral QDs were prepared by using $SBPIL_{\mathbf{80\%}}$ (80% conversion efficiency).

To verify the influence of spatial charge configuration on QD-cell interactions *in vitro*, nonspecific binding of zwitterionic QDs (SBPIL QDs and CBPIL QDs) with cultured HeLa cells was evaluated. Previous reports[12] predict neutral and hydrophilic QDs ($SBPIL_{80\%}$ QDs and $CBPIL_{100\%}$ QDs) to exhibit minimal cell binding. Instead, cells incubated with $SBPIL_{80\%}$ QDs and $CBPIL_{100\%}$ QDs displayed a significant increase of fluorescence signal suggesting nonspecific binding of the QDs to cells (Figure 2a–b, Supplementary Fig. S13). In addition, dramatic differences in nonspecific cell binding were observed depending on the betainization efficiencies of the SBPILs (Figure 2a).

The results with SBPIL QDs illustrate that, even for QDs that are neutral or slightly charged, the number of spatially exposed amines, i.e. positively charged groups, is an important factor that determines the level of nonspecific binding to cells. $SBPIL_{80\%}$ QDs possessing free tertiary amines (non-converted amines) exhibited significant nonspecific binding to cells despite the zero net charge of the particle, while $SBPIL_{100\%}$ QDs with no free amines showed virtually no binding to cells despite their small negative charge.

The results with CBPIL QDs reinforce the importance of the absence of positively charged groups on the outermost layer to achieve minimal nonspecific cell binding. Even though the chemical structure of $CBPIL_{100\%}$ indicates that the tertiary amine groups are fully converted to carboxybetaine moieties and thereby well screened by negative carboxylate groups, quaternary amines are more likely to be in the outermost layer (exposed) than carboxylate due to the affinity of carboxylate to the QD surface. The binding affinity of carboxylic acids to the QD surface is similar to that of imidazole groups, which are anchoring groups in BPILs[13]. Therefore, both carboxylic acids and imidazole moieties are expected to bind to the QD surface. Attraction of carboxylate groups towards the QD surface has been previously confirmed[14]. The high level of exposed amines resulted in significant nonspecific binding for $CBPIL_{100\%}$ QDs despite their nearly neutral charge (zeta potential of −0.3 mV), as shown in Figure 2b. $CBPIL_{100\%}$ QDs also exhibited strong interaction with diverse polymeric beads such as sephadex, superpose, sephacryl and superdex. In contrast, in the case of $SBPIL_{100\%}$ QDs, the quaternary amines are well screened from the environment by the sulfonates as sulfonate groups do not interact with the QD surface. Minimal nonspecific binding was observed for $SBPIL_{100\%}$ QDs.

Previous studies on gold surfaces (both nanoparticles and flat substrates) coated with carboxybetaineligands[15] also confirm our observation that spatially exposed positive charges trigger the high level of nonspecific binding. Unlike for $CBPIL_{100\%}$ QDs, carboxybetaine ligands are anchored to the gold substrates *via* thiols. Since thiols have a far greater binding affinity to gold than carboxylate[16], the entire carboxybetaine moieties are exposed to the environment, i.e. positive amine groups are well screened by negative carboxylate groups. Therefore, gold substrates coated with carboxybetaine ligands are reported to exhibit extremely low nonspecific binding properties (both to cells and proteins)[5e, 15b, 17].

The influence of the relative distribution of charges on the *in vivo* behavior of nanoparticles was further evaluated by analyzing the clearance of $SBPIL_{100\%}$ QDs versus $CBPIL_{100\%}$ QDs from the vessels of live mice. Upon retro-orbital injection, $SBPIL_{100\%}$ QDs that are likely to display negative chargeson their outermost layer cleared from vessels without leaving any evidence of nonspecific accumulation, while $CBPIL_{100\%}$ QDs are likely to display positive charge in their outermost layer clearly accumulated on vessels nonspecifically (Figure 2c–d).

Furthermore, we compared the *in vivo* binding and transport behavior of zwitterionic QDs versus non-ionic QDs to study the influence of the existence of charge in neutral

nanoparticles. $SBPIL_{100\%}$. QDs were chosen to represent zwitterionic QDs owing to their low nonspecific binding properties, and PEGPIL QDs were selected as an example of non-ionic QDs. Previously reported PEGPILs[10c] have the same polymer structure as BPILs except the water-solubilizing groups and therefore serve as an ideal control pair for BPIL QDs.

Nonspecific binding tests show that zwitterionic QDs exhibit slightly higher nonspecific binding to cells and serum proteins. As shown in Figure 3a, $SBPIL_{100\%}$ QDs exhibited slightly higher nonspecific cell adsorption than PEGPIL QDs at concentrations above 100 nM even though virtually no binding was observed for both $SBPIL_{100\%}$ QDs and PEGPIL QDs at the concentrations of 50 nM or lower. Also, when incubating with varying concentrations of fetal bovine serum (FBS), $SBPIL_{100\%}$ QDs exhibit weak nonspecific binding to serum proteins at high concentration of FBS (Supplementary Fig. S14), while a previous report on PEGPIL QDs show virtually no binding up to 0.90× serum[10c]. These results suggest that long, flexible, and non-ionic PEG chains are more effective than compact and ionic betaine groups at preventing bio-molecules from being adsorbed nonspecifically—they physically protect the surface better.

Plasma clearance data showed that zwitterionic QDs clear from blood significantly faster than non-ionic QDs. When zwitterionic QDs and non-ionic QDs ($SBPIL_{100\%}$ QD_{612} and PEGPIL QD_{570}) with similar net charge (−5.4 mV for PEGPIL QDs, −13.1mV for $SBPIL_{100\%}$ QDs) and hydrodynamic sizes (~10nm, Supplementary Fig. S16) were co-injected into mice, zwitterionic QDs cleared an order of magnitude faster than non-ionic QDs (Figure 3b, left panel). We confirmed that this result is solely due to the difference in the coatings and not due to the variability of the QD cores by measuring clearance kinetics of $SBPIL_{100\%}$ QD_{750} and PEGPIL QD_{750} (Figure 3b, right panel). The fast clearance of zwitterionic QDs might be due to an immune response triggered by weak nonspecific binding to serum proteins. Biodistribution analysis using inductively coupled plasma mass spectroscopy (ICP-MS) confirmsthe RES clearance of the particles; most of $SBPIL_{100\%}$ QDs is cleared through liver and spleen (Figure 3c and Supplementary Fig. S17).

Lastly, tumor transport measurements showed that non-ionic QDs extravasate from vessels and diffuse into tumor an order of magnitude faster than zwitterionic QDs displaying negative charged groups in their outermost layer. Transvascular transport of QDs in tumors was measured by calculating effective permeability[18] of the particlesin two different types of breast tumors: E0771 and MCaIV. The effective permeability measures the ability of QDs to extravasate from vessels and diffuse into the extravascular space, and is independent of clearance rate. Of the two breast tumor types, MCaIV has exceptionally large pores (pore cutoff size of 1.2 to 2 μm while most tumors show a pore cutoff size of 380 to 780 nm)[19]. In both tumor models, the zwitterionic QDs exhibited an effective permeability that was 1 to 2 orders of magnitude lower than non-ionic QDs (Figure 4). The unexpectedly low effective permeability of $SBPIL_{100\%}$ QDs is likely due to the combination ofthe exposed negative charge (the molecular arrangement of charges) and the weak negative net charge (net physical property) of $SBPIL_{100\%}$ QDs. Both the net negative charge and the exposed negative surface charge of SBPIL QDs may cause the QDs to be repelled from endothelial cells, which are known to display negative charge on their surface[20]. It is striking that the combination of different charge configurations and a small difference in the net charge (−5.4 mV versus −13.1 mV) yield significantly different transport behavior.

In this study, we designed and synthesized a new class of zwitterionic QD ligands (BPILs) to prepare neutral QDs with modulated spatial charge arrangements. Greatly enhanced stability and the low bio-fouling of BPIL QDs allowed an in-depth analysis of *in vivo* behavior. Our study demonstrates the critical importance of spatial charge arrangements in

determining *in vivo* characteristics of nanoparticles. Zwitterionic QDs displaying positive charges in their outermost layer exhibit nonspecific accumulation to cultured cells and vessels in live mice whereas zwitterionic QDs displaying negative charges in their outermost layer show minimal nonspecific adsorption. In addition, comparison of *in vivo* behavior between zwitterionic QDs and non-ionic QDs illustrate that exposed charged groups cause an enhanced interaction of zwitterionic QDs with their environment and result in significantly different binding and transport behavior *in vivo*. Therefore, when designing nanoparticles for *in vivo* applications, the three-dimensional configuration of charges needs to be closely considered with specific applications in mind. For instance, to minimize nonspecific interaction of nanoparticles with their environment, positively charge groups need to be spatially screened. In addition, the development of new conjugation methods employing neutral functional groups is highly recommended for achieving nanoparticles with long blood circulation and rapid transvascular delivery. These findings on QDs can be extended to other substrates, inorganic particles, and polymeric nanoparticles that can be used as imaging agents or drug carriers.

Supplementary Material

Refer to Web version on PubMed Central for supplementary material.

Acknowledgments

The research work of the authors is supported by the U.S. National Institute of Health grants, P01-CA080124 (R.K.J and D.F.), R01-CA085140 (R.K.J.), R01-CA096915 (D.F.), R01-CA115767 (R.K.J.), R01-CA126642 (R.K.J.), U54-CA151884 (M.G.B.), Federal Share Proton Beam Program Income (R.K.J.), and T32-CA073479 (R.K.J.); by the MIT DCIF CHE-9808061, DBI-9729592; by the ISN W911NF-07-D-0004 (M.G.B); by Samsung Scholarship (H.-S.H.); by the NSF-MRSEC program DMR-0117795 via the use of its shared user facilities; and by DoD Breast Cancer Research Innovator award (W81XWH-10-1-0016 (R.K.J.). Also, we thank Julia Kahn for technical assistance.

References

1. a) Bruchez M, Moronne M, Gin P, Weiss S, Alivisatos AP. Science. 1998281:2013–2016. [PubMed: 9748157] b) Chan WCW, Nie S. Science. 1998281:2016–2018. [PubMed: 9748158] c) Delehanty JB, Bradburne CE, Susumu K, Boeneman K, Mei BC, Farrell D, Blanco-Canosa JB, Dawson PE, Mattoussi H, Medintz IL. Journal of the American Chemical Society. 2011133:10482–10489. [PubMed: 21627173] d) Pinaud F, Clarke S, Sittner A, Dahan M. Nat Meth. 20107:275–285.
2. a) LaVan DA, McGuire T, Langer R. Nat Biotech. 200321:1184–1191.b) Brigger I, Dubernet C, Couvreur P. Advanced Drug Delivery Reviews. 200254:631–651. [PubMed: 12204596]
3. Verma A, Uzun O, Hu YH, Hu Y, Han HS, Watson N, Chen SL, Irvine DJ, Stellacci F. Nature Materials. 2008; 7:588–595.
4. a) Han HS, Devaraj NK, Lee J, Hilderbrand SA, Weissleder R, Bawendi MG. Journal of the American Chemical Society. 2010132:7838–7839. [PubMed: 20481508] b) Devaraj NK, Upadhyay R, Haun JB, Hilderbrand SA, Weissleder R. Angew Chem Int Ed. 200948:7013–7016.c) Hein C, Liu XM, Wang D. Pharmaceutical Research. 200825:2216–2230. [PubMed: 18509602]
5. a) Liu W, Choi HS, Zimmer JP, Tanaka E, Frangioni JV, Bawendi M. J Am Chem Soc. 2007129:14530–14531. [PubMed: 17983223] b) Muro E, Pons T, Lequeux N, Fragola A, Sanson N, Lenkei Z, Dubertret B. Journal of the American Chemical Society. 2010132:4556–4557. [PubMed: 20235547] c) Holmlin RE, Chen X, Chapman RG, Takayama S, Whitesides GM. Langmuir. 200117:2841–2850.d) Chen S, Zheng J, Li L, Jiang S. Journal of the American Chemical Society. 2005127:14473–14478. [PubMed: 16218643] e) Ladd J, Zhang Z, Chen S, Hower JC, Jiang S. Biomacromolecules. 20089:1357–1361. [PubMed: 18376858]
6. a) Dabbousi BO, Rodriguez-Viejo J, Mikulec FV, Heine JR, Mattoussi H, Ober R, Jensen KF, Bawendi MG. J Phys Chem B. 1997101:9463–9475.b) Bruchez M Jr, Moronne M, Gin P, Weiss S,

Alivisatos AP. Science. 1998281:2013–2016. [PubMed: 9748157] c) Peng ZA, Peng X. J Am Chem Soc. 2001123:183–184. [PubMed: 11273619]

7. Xie J, Xu C, Kohler N, Hou Y, Sun S. Advanced Materials. 2007; 19:3163–3166.
8. Martin AL, Bernas LM, Rutt BK, Foster PJ, Gillies ER. Bioconjugate Chemistry. 2008; 19:2375–2384. [PubMed: 19053308]
9. Chithrani BD, Ghazani AA, Chan WCW. Nano Letters. 2006; 6:662–668. [PubMed: 16608261]
10. a) Nikolic MS, Krack M, Aleksandrovic V, Kornowski A, Förster S, Weller H. Angewandte Chemie International Edition. 200645:6577–6580.b) Geidel C, Schmachtel S, Riedinger A, Pfeiffer C, Müllen K, Klapper M, Parak WJ. Small. 20117:2929–2934. [PubMed: 21990195] c) Liu W, Greytak AB, Lee J, Wong CR, Park J, Marshall LF, Jiang W, Curtin PN, Ting AY, Nocera DG, Fukumura D, Jain RK, Bawendi MG. J Am Chem Soc. 2010132:472–483. [PubMed: 20025223]
11. Breus VV, Heyes CD, Tron K, Nienhaus GU. ACS Nano. 2009; 3:2573–2580. [PubMed: 19719085]
12. a) Ryman-Rasmussen JP, Riviere JE, Monteiro-Riviere NA. Nano Letters. 20077:1344–1348. [PubMed: 17408303] b) Cho EC, Xie J, Wurm PA, Xia Y. Nano Letters. 20099:1080–1084. [PubMed: 19199477] c) Verma A, Stellacci F. Small. 20106:12–21. [PubMed: 19844908]
13. Rempel JY, Trout BL, Bawendi MG, Jensen KF. The Journal of Physical Chemistry B. 2006; 110:18007–18016. [PubMed: 16956292]
14. a) Allen PM, Liu W, Chauhan VP, Lee J, Ting AY, Fukumura D, Jain RK, Bawendi MG. J Am Chem Soc. 2010132:470–471. [PubMed: 20025222] b) Medintz I, Uyeda H, Goldman E, Mattoussi H. Nat Mater. 20054:435–446. [PubMed: 15928695] c) Chen J, Song JL, Sun XW, Deng WQ, Jiang CY, Lei W, Huang JH, Liu RS. Appl Phys Lett. 2009; 94:153115.
15. a) Mahmud G, Huda S, Yang W, Kandere-Grzybowska K, Pilans D, Jiang S, Grzybowski BA. Langmuir. 201127:10800–10804. [PubMed: 21711048] b) Zhang Z, Chen S, Jiang S. Biomacromolecules. 20067:3311–3315. [PubMed: 17154457] c) Yang W, Zhang L, Wang S, White AD, Jiang S. Biomaterials. 200930:5617–5621. [PubMed: 19595457]
16. a) Amabilino DB, Feyter SD, Lazzaroni R, Gomar-Nadal E, Veciana J, Rovira C, Abdel-Mottaleb MM, Mamdouh W, Iavicoli P, Psychogyiopoulou K, Linares M, Minoia A, Xu H, Puigmartí-Luis J. Journal of Physics: Condensed Matter. 200820:184003.b) Wang GM, Sandberg WC, Kenny SD. Nanotechnology. 200617:4819.c) Kondoh H, Kodama C, Sumida H, Nozoyec H. J Chem Phys. 1999111:1175–1184.
17. Yang W, Xue H, Li W, Zhang J, Jiang S. Langmuir. 2009; 25:11911–11916. [PubMed: 19583183]
18. Brown EB, Campbell RB, Tsuzuki Y, Xu L, Carmeliet P, Fukumura D, Jain RK. Nature Medicine. 2001; 7:864–868.
19. a) Hobbs SK, Monsky WL, Yuan F, Roberts WG, Griffith L, Torchilin VP, Jain RK. Proceedings of the National Academy of Sciences. 199895:4607–4612.b) Chauhan VP, Stylianopoulos T, Martin JD, Popovic Z, Chen O, Kamoun WS, Bawendi MG, Fukumura D, Jain RK. Nat Nano. 20127:383–388.
20. a) Simionescu M, Simionescu N. Annu Rev Physiol. 198648:279–293. [PubMed: 3010814] b) Stylianopoulos T, Soteriou K, Fukumura D, Jain RK. Annals of Biomedical Engineering. in press.

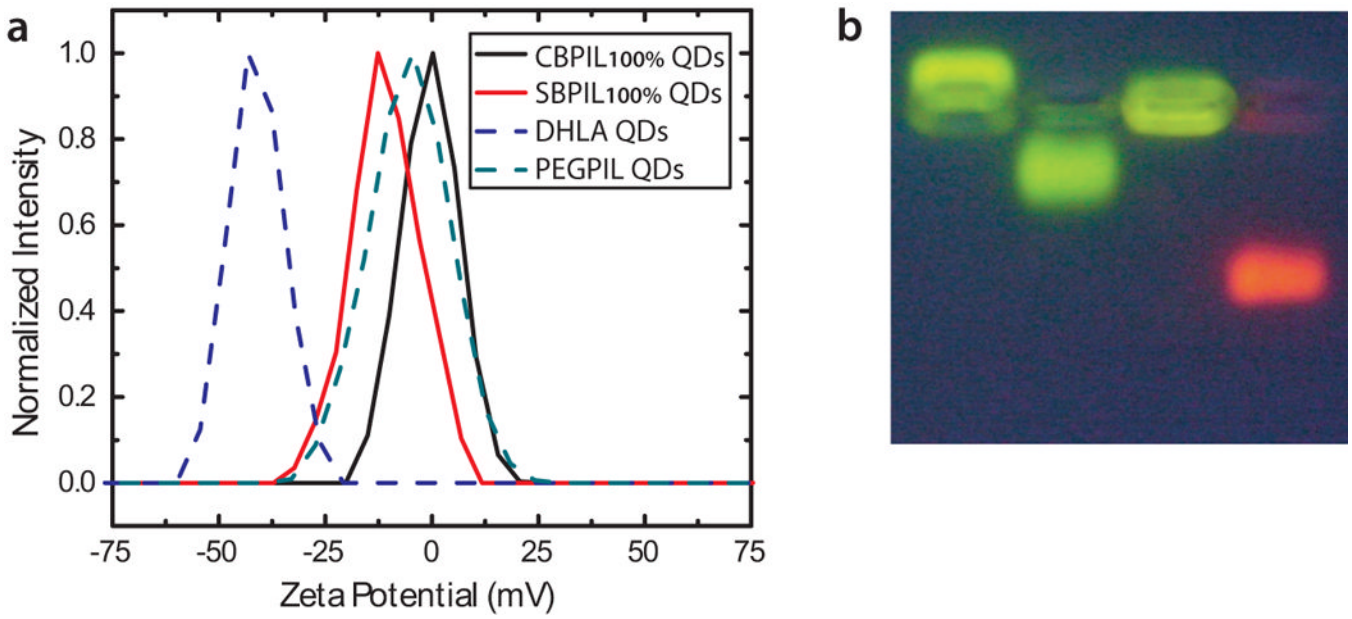

Figure 1.

Surface net charge measurements (a) Zeta potential measurements for SBPIL (red solid line) and CBPIL QDs (black solid line) illustrate that SBPIL QDs are slightly negative and CBPIL QDs are neutral. Zeta potential measurements for DHLA QDs (highly negative) and PEGPIL QDs (non-ionic QDs) are shown as a reference. (b) Gel electrophoresis of the PEGPIL QDs (first lane), SBPIL QDs (second lane), CBPIL QDs (third lane) and DHLA QDs (fourth lane) confirm the zeta potential measurement.

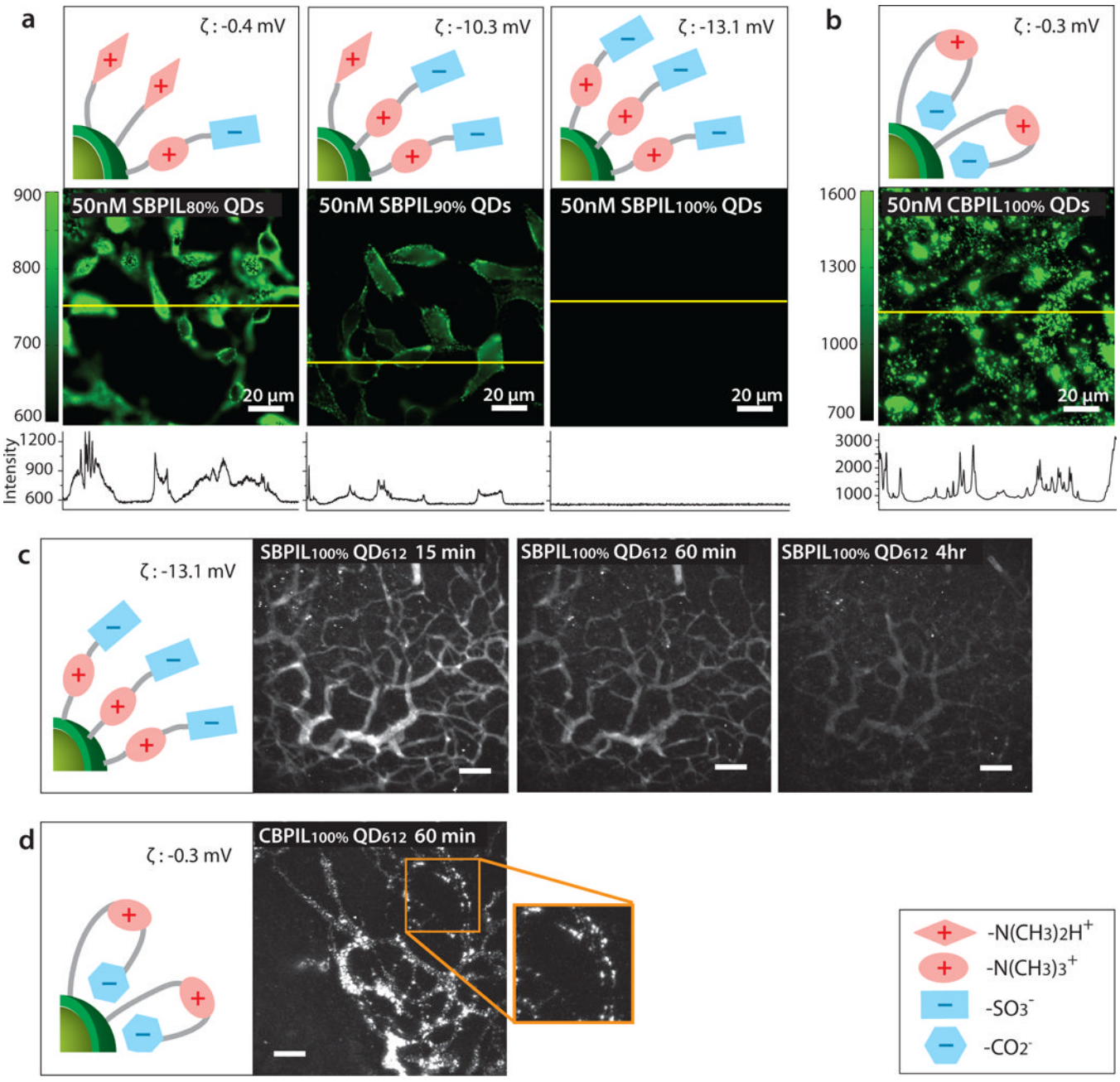

Figure 2.

Influence of charge distribution on nonspecific binding of QDs *in vitro* and *in vivo*. Cartoons of the QD surface are included to illustrate expected charge distribution on QDs for each sample. Charge distributions in the surface coatings were inferred from the different affinities of carboxylate groups and sulfonate groups towards QD surfaces. (a-b) Influence of surface charge distribution on nonspecific binding to HeLa cells. Exposure time = 100 ms.). Refer to Supplementary Fig. S12 for the images re-plotted using a heatmap for better visualization of the QD signal. (a) Significant decrease of the nonspecific binding is observed as the betainization efficiencies increases from 80% to 100% for SBPIL QDs. The data show that exposed free amines (positively charged groups) trigger nonspecific binding to cells. (b) $CBPIL_{100\%}$ QDs exhibit a high level of nonspecific binding due to exposed

amine groups. $CBPIL_{100\%}$ QDs display significantly higher nonspecific binding to cells than SBPIL QDs. Hence, the necessary change in the intensity scale of the plot below the picture was made. (c-d) Influence of charge distribution on *in vivo* clearance. (c)Clearance of SBPIL QD_{612} from the vessels. The vessels of E0771 murine mammary adenocarcinoma grown in SCID mice were imaged by multiphoton microscopy through a mammary fat pad window at 15 minutes, 60 minutes, and 4 hours after intravenous injection. Note that SBPIL QD_{612} clears from the vessels without leaving any evidence of nonspecific accumulation. Scale bar = 100 μm. (d) Clearance of $CBPIL_{100\%}$ QDs from the vessels. An image taken at 60 minutes after the injection of $CBPIL_{100\%}$ QDs illustrates that $CBPIL_{100\%}$ QDs accumulate on the vessel walls nonspecifically.

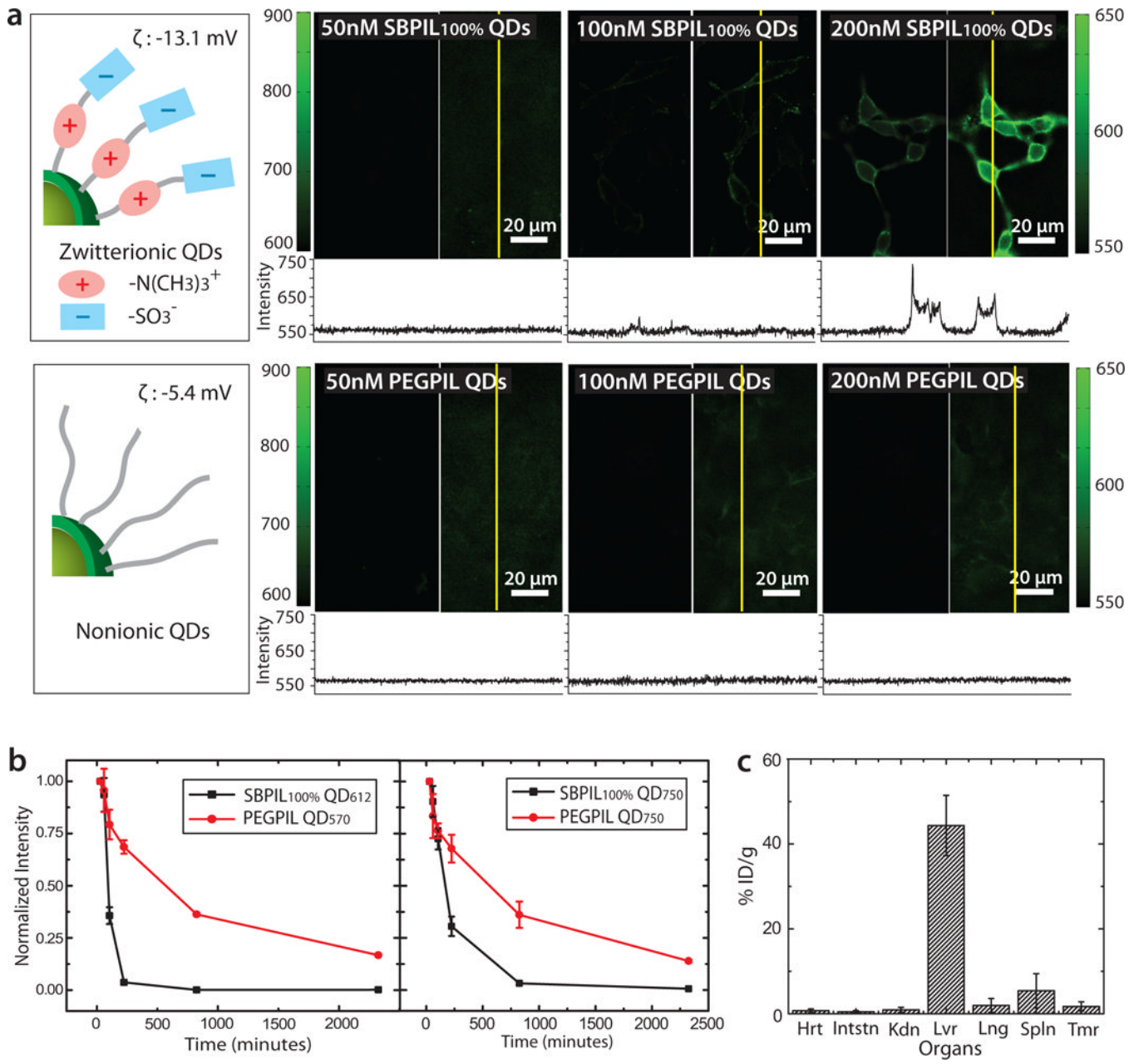

Figure 3.

Comparison of *in vivo* behavior of zwitterionic QDs *versus* non-ionic QDs. (a) Comparison of nonspecific binding to HeLa cells. Zwitterionic QDs exhibited slightly higher nonspecific cell binding than non-ionic QDs. Even though virtually no binding is observed for $SBPIL_{100\%}$ QDs at 50nM or lower, the level of nonspecific binding increases with higher concentrations of QDs (top). In contrast, the level of nonspecific binding for PEGPIL QDs remains minimal up to 200nM (bottom). Refer to Supplementary Fig. S12 for the images re-plotted using a heatmap for better visualization of the QD signal. (b) Comparison of **clearance kinetic**. Clearance kinetic of SBPIL QD_{612} and PEGPIL QD_{570} (left panel), which have very similar hydrodynamic diameters, and SBPIL QD_{750} and PEGPIL QD_{750} (right panel), that were synthesized with the same QD cores. Both results illustrate that SBPIL QDs clear from the vessels much faster than PEGPIL QDs (c) Bio distribution (%ID/

g tissue) of zwitterionic QDs 24 hours after QD injection. SBPIL QDs are cleared through liver and spleen, which may indicate RES clearance. Error bars represent 95% confidence interval.

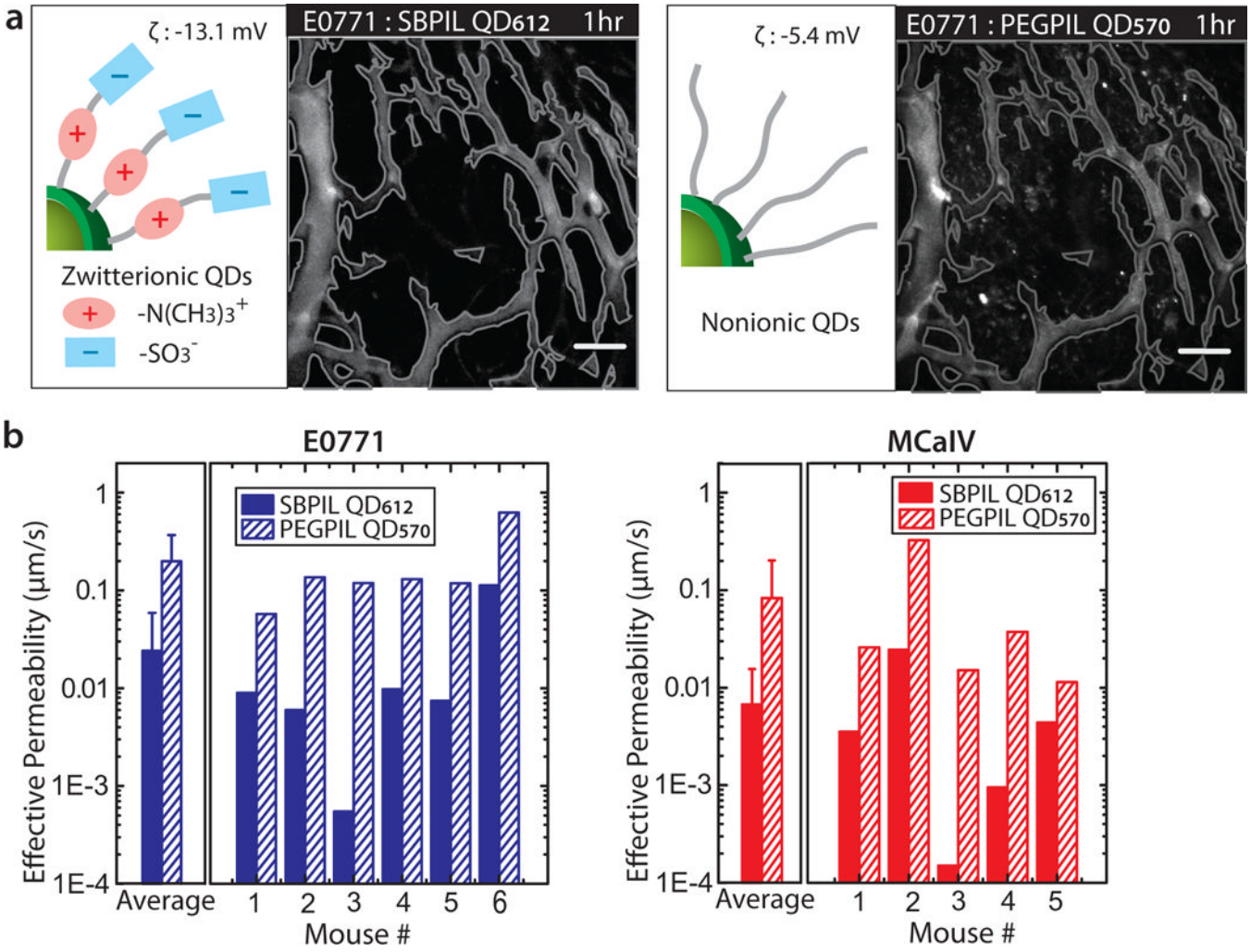

Figure 4.

Comparison of transvascular transport of zwitterionic QDs versus non-ionic QDs in breast cancers. (a) Real-time intravital microscopy of ligand-dependent nanoparticle distribution in a murine breast tumor. A mixture of$SBPIL\ QD_{612}$ (left panel) and $PEGPIL\ QD_{570}$ (right panel), which has the same hydrodynamic diameter, was injected intravenously into a SCID mouse bearing an E0771 murine mammary adenocarcinoma in a mammary fat pad chamber. Angiographic images demonstrate distribution of the nanoparticles one hour after injection. The initial fluorescence was recorded shortly after injection, and is depicted as the gray line. The images show that $SBPIL_{100\%}\ QD_{612}$extravasate from vessels significantly less than $PEGPIL\ QD_{570}$. Images are maximum intensity projections of 3D volumes. Scale bar is 100 μm. (b) Effective permeability of $SBPIL\ QD_{570}$ and $PEGPIL\ QD_{612}$ in mice bearing an E0771 murine mammary adenocarcinoma (left) and a MCaIV murine mammary adenocarcinoma (right). Solid bars represent the values obtained with $SBPIL\ QD_{612.}$ Lined bars represent the values obtained with $PEGPIL\ QD_{570}$. Error bars represent 95% confidence interval. In both tumor models, $SBPIL\ QD_{612}$ always showed significantly smaller effective permeability than $PEGPIL\ QD_{570}$.

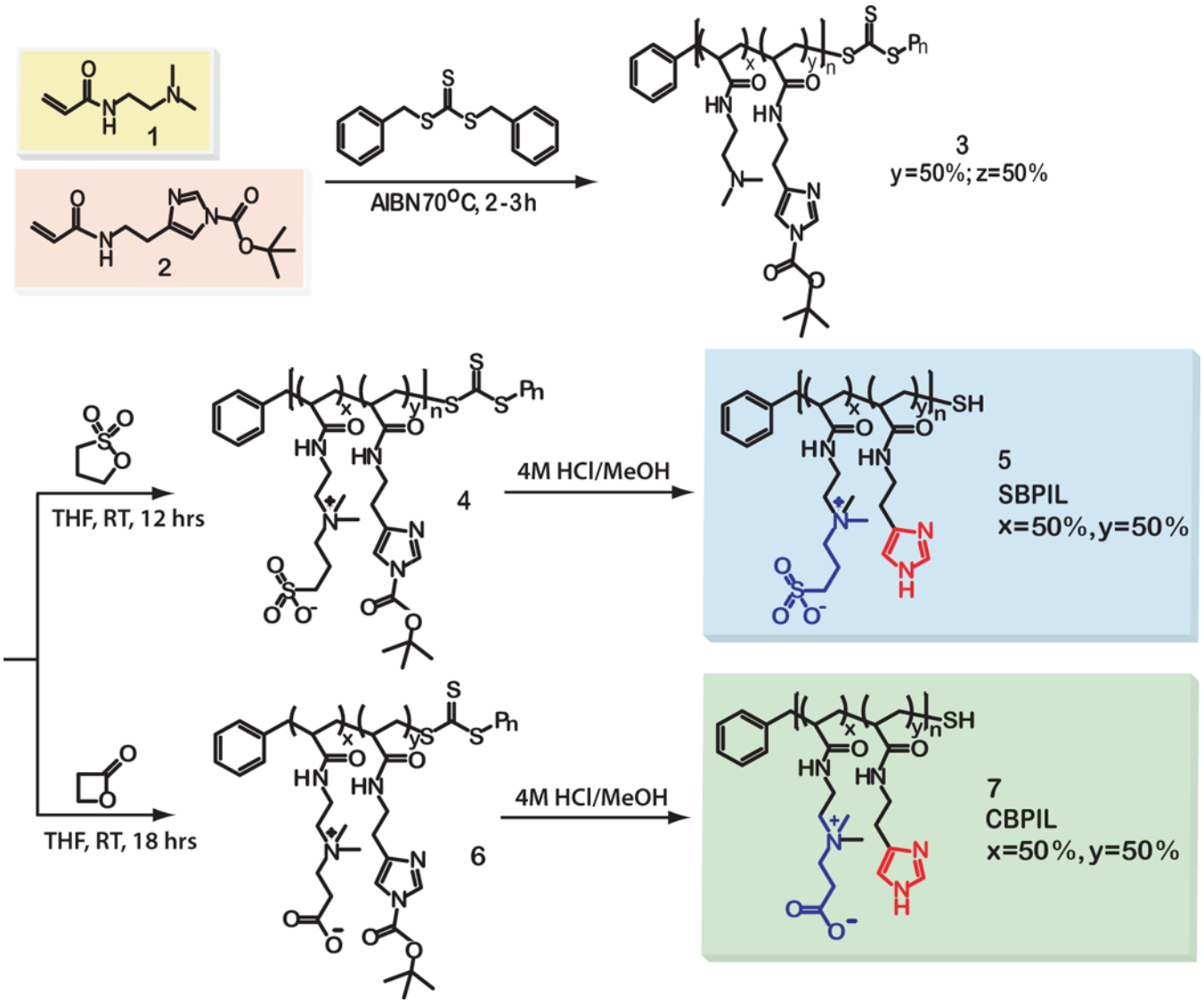

Scheme 1.

Schemes for synthesis of sulfobetaine and carboxybetaine functionalized poly (imidazole) ligands (SBPIL and CBPILs). Random copolymer backbones (3) are synthesized *via* radical addition fragmentation chain transfer (RAFT) mediated polymerization and betainized using 1,3-propanesultone and β-propiolactone to yield SBPILs (5) and CBPILs (7), respectively.